Chinese Chemical Letters 35 (2024) 109284

Contents lists available at ScienceDirect

Chinese Chemical Letters

journal homepage: www.elsevier.com/locate/cclet

Re-evaluating the nano-sized inorganic protective layer on Cu current collector for anode free lithium metal batteries

Shuo Zhang[a,b], Haitao Liao[c], Zhi-Qun Liu[b], Chong Yan[b,d,*], Jia-Qi Huang[b]

[a] School of Materials Science & Engineering, Beijing Institute of Technology, Beijing 100081, China
[b] Advanced Research Institute of Multidisciplinary Science, Beijing Institute of Technology, Beijing 100081, China
[c] Wuxi Yiwen Microelectronics Technology Co., Ltd., Wuxi 214000, China
[d] Shanxi Research Institute for Clean Energy, Tsinghua University, Taiyuan 030032, China

ARTICLE INFO

Article history:
Received 4 October 2023
Revised 27 October 2023
Accepted 6 November 2023
Available online 9 November 2023

Keywords:
Anode free lithium metal battery
Solid electrolyte interphase
Nano-sized protective layer
Lithium fluoride
Li deposition behavior

ABSTRACT

Anode free lithium metal batteries (AF-LMBs) have conspicuous advantages both in energy density and the compatibility of battery manufacturing process. However, the limited cycle life of AF-LMBs is a crucial factor hindering its practical application. Fluorinated or nitride artificial inorganic solid electrolyte interphase (SEI) has been found as an effective method to prolong the lifespan of AF-LMBs. Herein, by investigating the impact of nano-sized inorganic gradient layers (LiF or Li_3N) on initial Li deposition behavior, we notice that the Li^+ diffusion barrier and the deposition morphology are highly depended on the thickness of inorganic layers. Thicker protective layers cause larger overpotential as well as more aggregated Li^+ distribution. This study reveals that the ideal SEI should be synthesized thin and uniformly enough and uncontrollable artificial SEI can cause damage to the lifespan of AF-LMBs.

Due to the limitation of intercalation mechanism, lithium (Li) ion batteries, usually with graphite as anode, have been approaching its theoretical energy density [1,2]. As a result, Li metal batteries have been widely investigated due to its high theoretical capacity (3860 mAh/g) and lowest reduction potential (−3.04 V *vs.* standard hydrogen electrode) and regarded as the ultimate choice for next generation high energy density rechargeable batteries [3–5]. The energy density can be further improved when current collectors are used as anodes to construct anode free lithium metal batteries (AF-LMBs) [6–9]. AF-LMBs are better compatible with existing production systems and have more friendly requirements for the manufacturing environment than lithium metal batteries due to the absence of lithium metal. However, the commercial deployment of AF-LMBs is postponed by their poor cycling performance, which is related to the notorious electrode/electrolyte interface [10–13]. The stability of the interface is crucial for leveraging the high energy density of AF-LMBs [14].

Specifically, electrolytes will be reduced at the anode surface to form a solid electrolyte interphase (SEI) that allows the conduction of Li^+ while insulating electrons [15–18]. An ideal SEI should have a proper thickness as well as excellent mechanical and chemical stability [19,20]. Nevertheless, because of the high reactivity of Li, natural SEI undergoes continuous thickness increasement to protect the electrode, which undoubtedly consumes capacity [21]. Optimizing the composition of the electrolyte is one of the most direct methods to adjust the properties of the SEI [22–24]. What is more, the construction of artificial SEI is also a commonly used approach in the research community [25–31].

Natural SEI usually has a double-layer structure, with an inner inorganic layer and an outer organic layer [32]. In detail, LiF and Li_3N, as the common inorganic components, are considered as powerful support for the SEI stability [33–37]. As discussed by Fan *et al.*, LiF can effectively inhibit the growth of dendritic Li thanks to its high bulk modulus (70 Gpa) and interfacial energy (73.28 meV/Å^2) [38]. Besides, the large band gap of LiF can block the electron transfer from Li to SEI, which provides sufficient protection for Li through preventing side reactions between Li and electrolyte [39]. Commonly, Li^+ can transport through the grain boundary of LiF since it exhibits an extremely low bulk conductivity [40,41]. In contrast, Li_3N delivers the lowest Li^+ bulk diffusion barrier among the common inorganic components in SEI, including LiF, Li_2O and Li_2CO_3 [42]. It is worth noting that although many researchers prepare LiF or Li_3N layers on electrode surfaces through artificial means to improve the cyclic performance, the thickness of these layers far exceeds the actual SEI observed through cryo-transmission electronic microscopy [43,44].

* Corresponding author.
E-mail address: yanc@bit.edu.cn (C. Yan).

https://doi.org/10.1016/j.cclet.2023.109284
1001-8417/

This undoubtedly increases the difficulty of Li^+ transportation, making it difficult to replicate lithium deposition behavior under real operating conditions. By further reducing the thickness of the inorganic layer in SEI, we can gain deeper insights into the lithium deposition morphology caused by ultra-thin inorganic layers. This will also help us better understand the crucial role played by inorganic components such as LiF and Li_3N in the SEI.

Herein, we obtained gradient thickness LiF and Li_3N film layers through thermal evaporation method with the film thickness controlled below 15 nm. Focusing on the initial lithium deposition behavior during discharge in Li|Cu half cells, we observed that the increasement of nano-sized film thickness promoted the monotonical rise in the nucleation overpotential of Li. However, this was inconsistent with the morphology evolution trend observed through scanning electron microscope (SEM) from a thermodynamic perspective. The non-uniform distribution of the inorganic layer in thickness is the main reason for the island-like deposition morphology of Li. This contradicts with the common reports, providing new insight into the development of stable SEI design strategies for AF-LMBs.

Silicon wafer (Si) and copper (Cu) were selected as substrates and evaporated with LiF (Fig. S1 in Supporting information). Compared with Cu, which is used as current collector, Si helps us calibrate the thickness of LiF accurately and observe the evaporated morphology of LiF clearly owing to its high surface flatness. As shown in Fig. 1, we marked the thickness of LiF layer through atomic force microscope (AFM) owing to its availability to characterize the nanoscale surface morphology as well as film thickness. The difference in height caused obvious color discrimination on each side of the image in Figs. 1a-c. What is more, the variation of cross-section height showed the thickness of LiF layer intuitively, which was 5 nm, 10 nm and 15 nm, respectively (Figs. 1d–f). By narrowing the field of view, evaporation morphology of LiF layer was exhibited clearly, which covered the Si substrate homogenously (Figs. 1g-i). In detail, the surface roughness of 5 nm evaporation layer was 1.7 nm, while it was 3.37 nm for the 15 nm film. The surface roughness increased linearly with the raising of LiF layer thickness. Besides, surface morphology and component of inorganic layers was also observed through SEM and X-ray photoelectronic spectroscopy (XPS) with different substrates in Figs. S2 and S3 (Supporting information).

Based on the thickness calibration on Si, we obtained the gradient thickness LiF layer on Cu substrates to explore the relationship between LiF thickness and Li deposition morphology. The existence of LiF layer obviously increased the deposition resistance of Li. As shown in Fig. 2a, compared with bare Cu, LiF layer coated Cu showed a larger Li nucleation overpotential (η_n).

Further statistical analysis portrayed that the increase in LiF thickness led to a monotonic increase in η_n (Fig. 2b). The relationship between the surface roughness and nucleation overpotential was also exhibited. Different SEM images with varying deposition capacities demonstrated the evolution of Li deposition morphology in the early stages (Fig. 2c and Fig. S4 in Supporting information). At a capacity of 0.05 mAh/cm^2, corresponding to the onset of deposition, noticeable differences in the deposition morphology are observed for different thicknesses of LiF. Bare Cu and 5 nm LiF presented dendritic morphology (Fig. S5 in Supporting information). In contrast, island-like morphology appeared as LiF thickness increased. According to classical nucleation theory, there was a negative correlation between η_n and nucleus radius [45]. This implied that the nucleus radius of the 15 nm LiF layer should be the smallest, which obviously contradicted with what we observed through SEM. Based on the AFM images, LiF layer exhibited fluctuations in thickness. We believed that when LiF was thick enough, there was a noticeable redistribution of Li^+ concentration gradient on the electrode surface. In this scenario, Li^+ was more likely to diffuse through the thinner region of LiF, thereby increasing the nearby Li^+ concentration. Correspondingly, this resulted in the formation of large Li nucleus and subsequent deposition "hotspots", promoting the formation of island-like Li deposition morphology in that position. As the deposition capacity further raised to 0.1 mAh/cm^2, the coverage of Li on the Cu surface also increased. SEM images showed that different island-like Li crystal nucleus in the 15 nm LiF layer were connected by dendrites, further reducing the differences in deposition morphology between different LiF layers. This phenomenon was also observed in the second deposition (Fig. S6 in Supporting information). It indicated that the presence

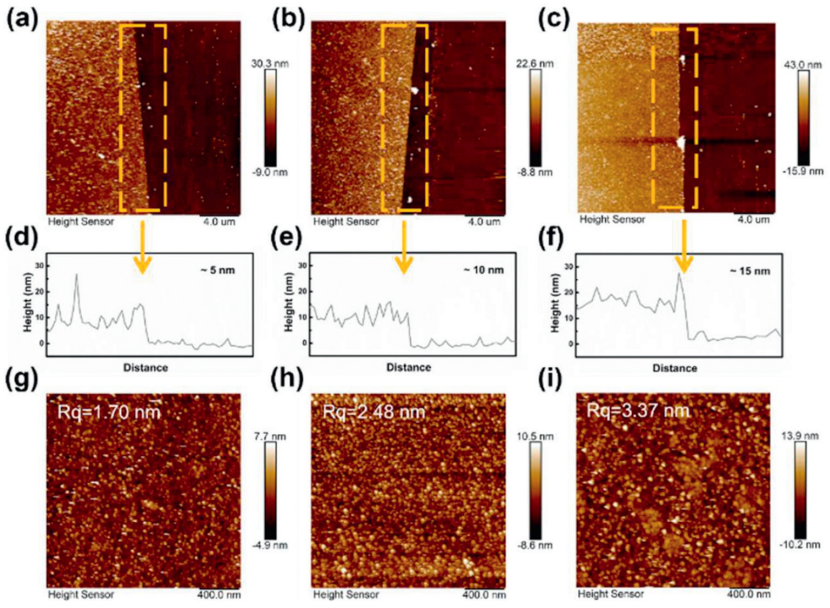

Fig. 1. AFM images of nano-sized LiF films deposited on Si substrates. (a-c) Thickness measurements over 20×20 μm^2 area under different thermal evaporation conditions. Corresponding height profile for (d) 5 nm, (e) 10 nm, (f) 15 nm LiF films. (g-i) Surface morphology of LiF films with different thickness over 2×2 μm^2 area.

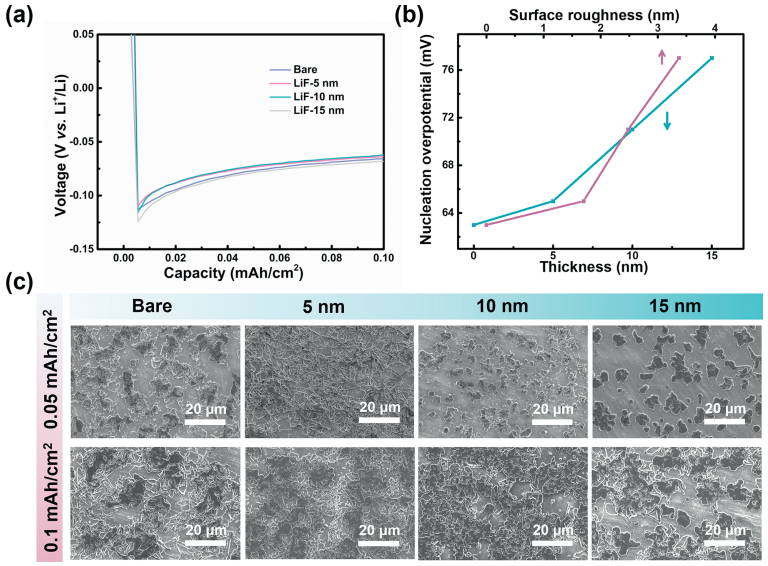

Fig. 2. Li plating behavior under LiF films in different Li|Cu half cells. (a) Experimental voltage curves of Li deposition on Cu substrates covered by gradient thickness of LiF films. (b) The relationship between the LiF thickness and nucleation overpotential. (c) SEM images of Li plating layer with progressive deposition capacity and different LiF thickness.

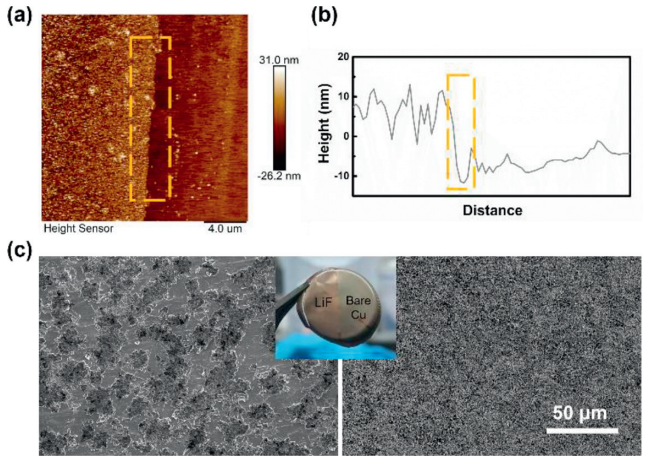

Fig. 3. Li plating behavior in the same Li|Cu half cells with half of Cu current collector covered by LiF film. AFM height image of the LiF film on (a) Si substrate and (b) specific height profile. (c) SEM images of the deposited Li on Cu covered by LiF (left) and bare Cu (right), and the insert was the optical photograph of Cu surface after 0.1 mAh/cm^2 Li deposited.

of the LiF layer did not fundamentally change the deposition behavior of lithium, at least for a 5 nm LiF layer.

In order to minimize the error caused by slight differences in the electrochemical processes of different batteries, we used a copper foil with half part covered by a 15 nm LiF layer and the other side bare for Li deposition. Figs. 3a and b indicated the evaporation morphology and height profile of the half-covered LiF layer. Not surprisingly, as shown in Fig. 3c, Li more preferred depositing on the surface without LiF layer (right part of the inset picture), shining with metallic luster. The current collector was exposed on the LiF layer covered part, which implied less deposited Li. Furthermore, there were noticeable differences in the microscopic deposition morphology of Li on the surface of aforementioned Cu. The surface of bare Cu was completely covered by layers of dendritic Li deposition, while the LiF covered part presented an island-like deposition morphology. The results indicated that the coverage of LiF increased the diffusion resistance of Li^+, promoting its deposition on the bare Cu. Meanwhile, the presence of island-like Li deposition morphology caused by different thicknesses of LiF layer still existing, which solidified the validity and accuracy of the discussions described in Fig. 2.

What is more, we wondered the effect of other common inorganic nano-sized layer on Li deposition behavior. Hence, we chose Li_3N which had a high Li^+ bulk diffusion coefficient, in contrast to the extremely low Li^+ conductivity of LiF bulk. Additionally, we obtained the nanoscale Li_3N layers through thermal evaporation, with 5 nm and 10 nm thick. The surface morphology, surface roughness, and the cross-section thickness of Li_3N layer was spread out in Figs. S7 and S8 (Supporting information). Trustworthy, the increase in η_n was directly proportional to the raising of inorganic layer thickness (Fig. 4a and Fig. S9 in Supporting information). The Li deposition behavior on Li_3N layer was consistent with the overall trend of the LiF system at different deposition capacities (Fig. 4b). The island-like morphology was more obviously when the Li_3N thickness approached 10 nm. 0.05 mAh/cm^2 deposition capacity led to many island-like Li particles in the SEM images for the 10 nm Li_3N. However, instead of further enlarging of the Li islands, lots of dendrites appeared to connect different islands when the deposition capacity reached 0.1 mAh/cm^2, which could be clearly observed both in Fig. 4b and Fig. S10 (Supporting information). Meanwhile, CE measurement was adopted to evaluated the cyclic performance of Li, whether bare Cu, LiF layer and Li_3N layer could work in large time scale shown in Fig. 4c. Based on the overall trend of changes, it was clear that the application of the nano-sized inorganic layers as well as the thickness of these layers did not significantly affect the long-term stability of the batteries. The average CE remained around 99.2% for all systems. Same results were also obtained in Fig. S11 (Supporting information).

In this contribution, we prepared nano-sized gradient thickness LiF/Li_3N layers through thermal evaporation to re-evaluate its influence on Li deposition behavior (Fig. 5). The nano-sized inorganic layer increased the difficulty of Li^+ diffusion, forcing Li^+ to concentrate and diffuse through the thinner areas of the inorganic layer, forming island-like deposition morphology. However, this deposition morphology would only appear at the very beginning of Li deposition, since Li dendrites filled in the blank areas to connect the island-like morphology subsequently. The uniformity of inor-

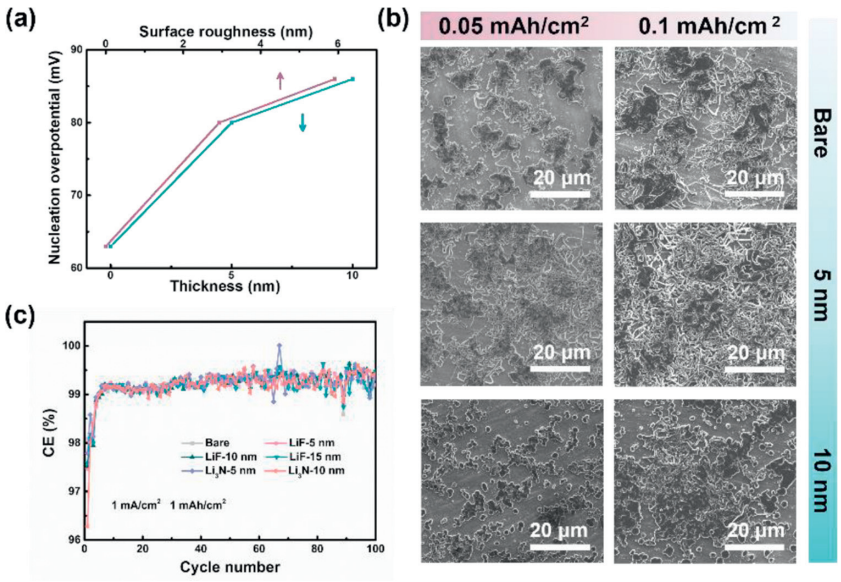

Fig. 4. Li plating behavior under gradient thickness Li_3N films. (a) The relationship between Li_3N thickness and nucleation overpotential. Surface roughness was also considered as a key variate. (b) SEM images of Li nucleus layer under different thickness Li_3N layer and Li deposition capacity. (c) Cycling performance of Li|Cu cells with gradient LiF/Li_3N thickness.

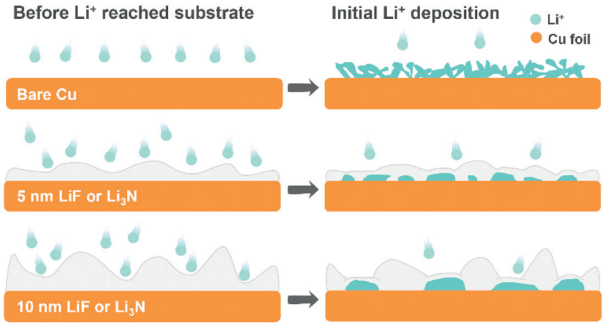

Fig. 5. A schematic illustration of the initial Li deposition behavior with the nano-sized LiF or Li_3N layer. Li^+ inclined to accumulate on the thinner area of the inorganic layer when approaching the electrode surface and exhibited an island-like deposition morphology.

ganic layers largely adjusts initial Li deposition morphology which should be considered when artificial SEI is designed for AF-LMBs.

Declaration of competing interests

The authors declare that they have no known competing financial interests or personal relationships that could have appeared to influence the work reported in this paper.

Acknowledgments

This work was supported by the National Natural Scientific Foundation of China (No. 22379014) and Shanxi key research and development program (No. 202102060301011). We thank Jun-Fan Ding, Xiao-Qing Ding, Ye Xiao, Lei Xu, Yi Yang and Yu-Xing Yao for technical support and discussions.

Supplementary materials

Supplementary material associated with this article can be found, in the online version, at doi:10.1016/j.cclet.2023.109284.

References

[1] Y. Yang, L. Xu, C. Yan, et al., Energy Lab 1 (2022) 220011.
[2] F. Luo, B. Liu, J. Zheng, et al., J. Electrochem. Soc. 162 (2015) A2509–A2528.
[3] D.C. Lin, Y.Y. Liu, Y. Cui, Nat. Nanotechnol. 12 (2017) 194–206.
[4] G.M. Hobold, J. Lopez, R. Guo, et al., Nat. Energy 6 (2021) 951–960.
[5] X.Z. Fan, M. Liu, R. Zhang, et al., Chin. Chem. Lett. 33 (2022) 4421–4427.
[6] J. Qian, B.D. Adams, J. Zheng, et al., Adv. Funct. Mater. 26 (2016) 7094–7102.
[7] S. Nanda, A. Gupta, A. Manthiram, Adv. Energy Mater. 11 (2020) 2000804.
[8] R.V. Salvatierra, W. Chen, J.M. Tour, Adv. Energy Sustain. Res. 2 (2021) 2000110.
[9] B. Wu, C. Chen, L.H.J. Raijmakers, et al., Energy Stor. Mater. 57 (2023) 508–539.
[10] R. Weber, M. Genovese, A.J. Louli, et al., Nat. Energy 4 (2019) 683–689.
[11] A.J. Louli, A. Eldesoky, R. Weber, et al., Nat. Energy 5 (2020) 693–702.
[12] C. Jin, T. Liu, O. Sheng, et al., Nat. Energy 6 (2021) 378–387.
[13] C.J. Huang, B. Thirumalraj, H.C. Tao, et al., Nat. Commun. 12 (2021) 1452.
[14] J. Chen, X. Fan, Q. Li, et al., Nat. Energy 5 (2020) 386–397.
[15] E. PELED, J. Power Sources 9 (1983) 253–266.
[16] S. Zhang, M.S. Ding, K. Xu, et al., Electrochem. Solid-State Lett. 4 (2001) A206–A208.
[17] Z. Zhang, Y. Li, R. Xu, et al., Science 375 (2022) 66–70.
[18] R. Xu, C. Yan, J.Q. Huang, Trend. Chem. 3 (2020) 5–14.
[19] X.B. Cheng, R. Zhang, C.Z. Zhao, et al., Chem. Rev. 117 (2017) 10403–10473.
[20] C. Yan, R. Xu, Y. Xiao, et al., Adv. Funct. Mater. 30 (2020) 1909887.
[21] J.F. Ding, R. Xu, X.X. Ma, et al., Angew. Chem. Int. Ed. 61 (2021) e202115602.
[22] B. Horstmann, J. Shi, R. Amine, et al., Energy Environ. Sci. 14 (2021) 5289–5314.
[23] D. Luo, M. Li, Y. Zheng, et al., Adv. Sci. 8 (2021) e2101051.
[24] Y.X. Yao, X. Chen, C. Yan, et al., Angew. Chem. Int. Ed. 60 (2021) 4090–4097.
[25] R. Xu, X.B. Cheng, C. Yan, et al., Matter 1 (2019) 317–344.
[26] C. Yan, X.B. Cheng, Y.X. Yao, et al., Adv. Mater. 30 (2018) e1804461.
[27] R. Xu, X.Q. Zhang, X.B. Cheng, et al., Adv. Funct. Mater. 28 (2018) 1705838.
[28] J. Xie, L. Liao, Y. Gong, et al., Sci. Adv. 3 (2017) eaao3170.
[29] J. Ding, R. Xu, C. Yan, et al., Chin. Chem. Lett. 31 (2020) 2339–2342.
[30] Y. Xiao, R. Xu, C. Yan, et al., Sci. Bull. 65 (2020) 909–916.
[31] J.Y. Duan, J.X. Chen, F.F. Wang, et al., J. Energy Chem. 87 (2023) 473–478.
[32] D. Aurbach, J. Power Sources 89 (2000) 206–218.
[33] D. Lin, Y. Liu, W. Chen, et al., Nano Lett. 17 (2017) 3731–3737.
[34] W. Chang, J.H. Park, D.A. Steingart, Nano Lett. 18 (2018) 7066–7074.
[35] L. Chen, K.S. Chen, X. Chen, et al., ACS Appl. Mater. Interfaces 10 (2018) 26972–26981.
[36] N. Hornsveld, W.M.M. Kessels, R.A. Synowicki, et al., Phys. Chem. Chem. Phys. 23 (2021) 9304–9314.
[37] C. Yan, H.R. Li, X. Chen, et al., J. Am. Chem. Soc. 141 (2019) 9422–9429.
[38] X.L. Fan, X. Ji, F.D. Han, et al., Sci. Adv. 4 (2018) eaau9245.
[39] R. Xu, F. Han, X. Ji, et al., Nano Energy 53 (2018) 958–966.
[40] L. Benitez, J.M. Seminario, J. Electrochem. Soc. 164 (2017) E3159–E3170.
[41] T. Aashish, B.S. Mallik, J. Phys. Chem. C 123 (2019) 25015–25024.
[42] X.-X. Ma, X. Shen, X. Chen, et al., Small Struct. 3 (2022) 2200071.
[43] S. Liu, Y. Ma, J. Wang, et al., Chem. Eng. J. 427 (2022) 131625.
[44] J. Ko, Y.S. Yoon, Thin Solid Films 673 (2019) 119–125.
[45] A. Pei, G. Zheng, F. Shi, et al., Nano Lett. 17 (2017) 1132–1139.